GEOCHEMISTRY OF HYDROTHERMAL ORE DEPOSITS

Third Edition

Edited by

Hubert Lloyd Barnes
Ore Deposits Research Section
The Pennsylvania State University
University Park, Pennsylvania

John Wiley & Sons, Inc.
New York • Chichester • Weinheim • Brisbane • Singapore • Toronto

Chapter

5

Thermal Aspects of Ore Formation

LAWRENCE M. CATHLES III
Department of Geological Sciences, Cornell University

As the title of this book suggests, understanding the geochemistry of *hydrothermal* ore deposits involves understanding the interactions between hydrologic and thermal processes. Perhaps the most important thermal interaction is the advection of heat by water moving through a permeable porous or fractured lithic matrix in which there are temperature gradients. Water movement through temperature or other physical gradients (such as pressure or salinity) drives chemical change. For example, silica may be deposited if pore waters move from areas of higher to lower temperature because the solubility of silica is temperature dependent. Thus there can be a direct connection between fluid movement through temperature gradients and ore deposition. How much ore is deposited depends on how fast the thermal gradients move through the subsurface. Pore-fluid movements cause temperature gradients to migrate in the direction of fluid flow. The pore waters may be driven by the temperature gradients themselves (convection) or by an independent process. The important point is that fluid movements cause the subsurface temperature distribution to change if it is not uniform. Some of the strongest constraints on hydrothermal ore deposition are thermal.

The thermal aspects of ore formation can be investigated in a variety of ways. One way is to construct coupled numerical computer models of temperature and fluid flow and simulate the evolution of geologic systems of

interest. A great deal can, and has been, learned from such simulations, and more will be learned as chemical change is coupled with temperature and fluid flow. Simulations are very useful in checking more intuitive methods. Examples of recent reviews of this approach are available from a number of authors (Cathles, 1977, 1983, 1990; Norton and Knight, 1977; Norton and Taylor, 1979; Garven and Freeze, 1984a,b; Norton, 1984, 1988; Bethke, 1986; Bethke and Marshak, 1990; Bethke et al., 1991; Burrus et al., 1991; Furlong et al., 1991; Hanson, 1992; Person and Garven, 1992). Computer simulations have the disadvantage, however, that most geologists have neither ready access to computers nor the detailed knowledge of the software that is required to make such simulations. Also, the computer simulations are often complex enough in their own right that fundamental insights and understanding are difficult to extract.

Another approach that can help interpret either ore deposits or computer simulations is to constrain important aspects of the ore-forming process with simple calculations that can be carried out with paper and pencil. Calculations of this sort are often included in computer simulation papers, are exceptionally useful, and in some cases can be geologically more realistic than large-scale simulations because the analysis can be focused specifically on critical aspects of the problem. Hand calculations are basically of two kinds: those that calculate the thermal consequences of fluid flow and those that define its magnitude. Combining the two is particularly powerful. This chapter compiles paper and pencil tools the author has found useful and illustrates their use by applications to several kinds of hydrothermal ore deposits.

THERMAL CONSEQUENCES OF SUBSURFACE FLUID FLOW

The interaction between temperature and subsurface fluid flow is governed by a conservation-of-energy equation that may be written

$$\rho_m C_m \frac{\partial T}{\partial t} = A - \rho C J \cdot \nabla T + K_m \nabla^2 T \qquad (5.1)$$

where ρ_m and C_m are the density and heat capacities of the media (rock plus pore fluid) in g/cm^3 and cal/g-°C, respectively, ρ and C are the density and heat capacity of the pore fluid in the same units, T is the temperature in °C of the pore fluid and immediately adjacent rock (assumed to be the same), J is the Darcy velocity, superficial velocity, or volume flux (all equivalent expressions for J) of the pore fluid in cm/s, K_m is the thermal conductivity of the media (rock and pore fluids) in cal/cm-s-°C, A is the rate of heat generation in cal/cm^3-s, and ∇ is the Laplacian operator.

The Darcy velocity, J, deserves special comment. It is not really a velocity with dimensions of cm/s at all but a volume flux with dimensions of

cm^3/cm^2-s. It is the number of cubic centimeters of pore water that pass a 1-cm^2 section perpendicular to the flow per second. The Darcy flux, as we shall call it henceforth, is the velocity the pore fluid would have if it occupied the entire space instead of the space represented by the pores through which water is moving in the porous medium. Because the moving water occupies only the flowing porosity, ϕ_f, the true velocity of the pore water is J/ϕ_f.

It has been assumed in equation (5.1) that the pore fluid is incompressible (e.g., $\nabla \cdot J = 0$), and that ρC is constant. These are useful and nonrestrictive assumptions. Term by term, equation (5.1) states that the change of heat in a unit volume of the porous medium over a time, dt (first term on the left), equals the heat generated within that volume over dt (first term to the right of the equal sign), plus the heat advected into the volume by fluid flow, plus the net heat conducted into the volume (last term on right).

Migrating Thermal Fronts

Heat advection can be investigated with equation (5.1) by switching to a coordinate system that moves with thermal anomalies. Subsurface temperature will, in general, vary so that temperature is a function of spatial position and time. Symbolically we write $T = T(\mathbf{x}, t)$, where $\mathbf{x}$ is the position vector with components of x_1 along the x axis lying in the $\hat{\mathbf{i}}$ direction, and so on, so that $\mathbf{x} = x_1\hat{\mathbf{i}} + x_2\hat{\mathbf{j}} + x_3\hat{\mathbf{k}}$. Because T depends on both $\mathbf{x}$ and t, the total derivative of T follows from the chain rule. The total change in T equals the partial change in T with respect to t, at a fixed location in space, multiplied by the incremental change in t, plus the partial change in T with respect to space, at a particular instant of time, multiplied by the change in spatial location with time, multiplied by the incremental change in time:

$$DT(\mathbf{x}, t) = \left(\frac{\partial T}{\partial t}\right)_{x_i=\text{const.}} Dt + \left(\frac{\partial T}{\partial x_i}\right)_{t=\text{const.}} \left(\frac{\partial x_i}{\partial t}\right)_{t=\text{const.}} Dt$$

Rearranging and letting $(\partial x_i/\partial t)_{t=\text{const.}} = \mathbf{v}$, this equation may be rewritten:

$$\frac{\partial T}{\partial t} = \frac{DT}{Dt} - \mathbf{v} \cdot \nabla T \qquad (5.2)$$

To understand equation (5.2), imagine an observer standing beside a moving train of refrigerator cars. If the temperature of a particular car changes, $DT/Dt \neq 0$. If the train is moving and the cars do not all have the same temperature so that $\mathbf{v} \cdot \nabla T \neq 0$, then the temperature of cars in front of a stationary observer will change. Suppose the train is traveling in the x direction at one car per minute, each car maintains constant temperature so that $DT/Dt = 0$, but the temperature in each adjacent car (in the pos-

itive x direction) increases at 1°C per car. Equation (5.2) then becomes $\partial T/\partial t = -v_x\, \partial T/\partial x$, and the temperature in the cars at the observer's location (Eulerian or spatially fixed coordinate) will decrease at a rate of 1°C per minute. If there was the same difference in temperature between cars but all cars were cooling at 1°C/min, that is, $DT/Dt = -1$, the change observed at a stationary location would be −2°C/min. If the observer rode on any particular car (e.g., moved with the fluid in a moving Lagrangian coordinate system), only the change in temperature in the car to which the observer was attached would be observed, in this case −1°C/min.

There is nothing particularly sacred about the exact form of the transformation expressed in equation (5.2). A coordinate system that follows thermal anomalies, rather than the fluid motion, can be selected, for example, by modifying equation (5.2) slightly so that

$$v = J \frac{\rho C}{\rho_m C_m} \tag{5.3}$$

and

$$\frac{\partial T}{\partial t} = \frac{DT}{Dt} - \frac{\rho C}{\rho_m C_m} J \cdot \nabla T \tag{5.4}$$

That equations (5.3) and (5.4) describe the movement of a coordinate system in which temperature anomalies are stationary can be seen by substituting equation (5.4) into equation (5.1). The result is

$$\rho_m C_m \frac{DT}{Dt} = A + K_m \nabla^2 T \tag{5.5}$$

Equation (5.5) states that if there is no heat generation ($A = 0$) and if thermal diffusion is ignored ($K_m = 0$), then *there is no change in temperature in the moving coordinate system we have chosen* (e.g., $DT/Dt = 0$). In other words, in the absence of thermal diffusion and heating, a temperature anomaly will be swept by fluid flow through the porous medium at $\rho C/\rho_m C_m$ times the Darcy flux of the fluid, J. If the observation grid moves at $(\rho C/\rho_m C_m)J$, any and all thermal anomalies will appear stationary. Since $\rho_m \approx 2.7$, $C_m \approx 0.2$, and $\rho C \approx 1$, the thermal anomalies will move at about $1/0.54 = 1.8$ times the Darcy flux. For a thermal anomaly migrating at 1.8 times the Darcy flux, the water/rock ratio after passage of the anomaly will be 0.54 cm^3 fluid/cm^3 rock, or about 0.2 g fluid/g rock.

If the flow porosity is 10 vol% of the sediment (or ~0.1% in the fractures of an igneous rock) and the true velocity of the fluid is thus 10 (or 1000) times the Darcy flux, the pore waters will move through the thermal anomaly at ~5 (or ~500) times the rate at which the thermal anomaly migrates.

The pore waters migrating from a hot area into cool country rock may

deposit silica and other minerals. The deposition will be small because the water/rock ratio is small so long as the thermal front is allowed to migrate. For example, taking into account both temperature and fluid density, the geologic solubility of quartz peaks at about 2500 ppm (Cathles, 1983). At a water/rock mass ratio of 0.2 the maximum silicification expected from a freely migrating thermal front is 0.5 wt %. More sophisticated computer simulations confirm this conclusion (Cathles, 1983).

A silicification of 0.5 wt % is disappointingly small and we arrive at a first conclusion of importance to hydrothermal ore deposition: significant *thermal* deposition of silica (or any other mineral, because other minerals are generally a great deal less soluble than silica) can be expected only where thermal anomalies are immobilized. Immobilization can occur where the thermal front reaches the surface, where there is fluid boiling and the temperature is constrained to follow the liquid–vapor curve of water, or in areas where cold fluids mix with hot ones. In such areas, significant amounts of silica and other minerals with prograde solubilities may be deposited as the result of temperature drop and other processes. But unless physical factors conspire to immobilize a thermal anomaly, only very minor amounts of material (silica or base metals) can be deposited as a result of temperature change by fluids moving through that anomaly. Note that we do not consider contrasts in rock reactivity and skarn formation here.

The approach outlined above is quite general. The thermal front migrates at a rate equal to the product of the Darcy flux times the ratio of the thermal storage capacity of the fluid to that of the solid plus pore water combined. Chemical fronts migrate according to the same principle. For example, warm water dissolves about 25 wt% NaCl. The salt dissolution front in a sandstone that has a density of 2.5 g/cm^3, contains 20 wt % salt, and has 10% porosity will move at about half the Darcy flux because the sandstone carries 0.525 g NaCl/cm^3 solid, whereas the fluid carries 0.25 g NaCl/cm^3 fluid. Under isothermal conditions, an oxygen isotopic front will migrate at about half the Darcy flux because water contains about 56 mol of oxygen per 1000 cm^3 of water, whereas rock contains about 100 mol of oxygen per 1000 cm^3 of rock. Hydrogen isotopic anomalies will migrate at about 18 times the Darcy flux because water contains about 111 mol of hydrogen per 1000 cm^3 of water, whereas rock contains only about 6 mol of hydrogen per 1000 cm^3 of rock. In each case the movement of the chemical front could be followed by substituting an expression similar to (5.3) and (5.4) into a conservation equation similar to (5.1). In each case the motion of the front would adequately be described by the average velocity, but diffusion and dispersion would smear the front out with time. The smearing by diffusion and dispersion is characterized by a Peclet number; further smearing due to finite reaction rates can be characterized by a Damkohler number. Examples and further discussion are available in the literature (Cathles, 1983; Lassey and Blatner, 1988; Blattner and Lassey, 1989; Banner and Hanson, 1990; Cathles and Shea, 1992).

In cases where the motion of an alteration front is tied to the motion of the thermal front, the magnitude of the initial alteration can be estimated. For example, knowing that the thermal front migrates with a water/rock ratio of 0.54 cm^3 fluid/cm^3 rock, that the equilibrium water/rock isotopic fractionation changes by ~10‰ between 350°C and 100°C, and that the ratio of oxygen concentrations in the water to that in the rock is 56/100 suggests that migration of a 350°C thermal front will enrich the rock downstream in ^{18}O by about 3‰ (= 0.54 × 0.56 × 10). The enrichment is actually greater than this because earlier enrichment enhances ^{18}O in the fluid and leads to a greater increase in ^{18}O in the rock as the anomaly migrates (Cathles, 1983). Nevertheless, simple thermal calculations determine the water/rock ratio that is effective in many kinds of alteration and allow the magnitude of alteration to be estimated.

Thermal Anomalies at the Surface

VERTICAL FLOW

A second very useful relationship can be deduced from equation (5.1). The steady-state temperature distribution near the surface can be determined, in the case where there are no thermal sources or sinks and the vertical outflow ($J_z > 0$) of water is known, by solving

$$\frac{\partial^2 T}{\partial z^2} = \frac{\rho C J_z}{K_m}\frac{\partial T}{\partial z} = -\frac{1}{\delta}\frac{\partial T}{\partial z} \qquad (5.6)$$

For convenience we have defined a skin depth $\delta = K_m/\rho C J_z$. Substituting a trial solution $T = e^{rz}$ results in the algebraic equation, $r^2 - (1/\delta)r = 0$, which has the solutions $r = 0$ and $r = 1/\delta$. The solution to equation (5.6) thus has the general form of $T = A + Be^{z/\delta}$. The boundary conditions $T(z = 0) = 0$ requires $A = -B$, and the condition that $T(z = L) = T_0$ requires $A = T_0/(1 - e^{-L/\delta})$. Thus

$$\frac{T}{T_0} = \frac{1 - \exp(z/\delta)}{1 - \exp(-L/\delta)} \qquad (5.7)$$

Plotting equation (5.7) shows that the vertical outflow is small, the thermal gradient increases linearly with depth, and the heat flow, J, equals $K_m T_0/L$. When the vertical fluid outflow is large and δ small, the temperature increases rapidly with depth to T_0 according to $T = T_0(1 - e^{z/\delta})$, and the heat flow, J, equals $K_m T_0/\delta$. Between a depth of ~2δ and L the temperature is constant and equal to T_0. Remember in these equations that depth is positive upward, and negative as one proceeds into the subsurface. This problem of geothermal gradients was first solved by Bredehoeft and Papadopolos (1965) and plots and additional discussion can be found there.

The concept of skin depth can be very useful. For example, trace-element distributions suggest that the upper 20 m of the Amulet Rhyolite at Noranda was originally a basalt that has been silicified. If the silicification reflects outflow and near-surface cooling, then $\delta \approx 20$ m and the fluid outflow, taking $K_m = 6 \times 10^{-3}$ cal/cm-s-°C, must have been about 94 g/cm^2-yr ($= K_m/\rho C\delta$). For $T_0 \approx 350$°C, heat flow over the silicified area was $T_0 K_m/\delta = (350)(6 \times 10^{-3})/(20 \times 10^2) \approx 1000\,\mu$cal/$cm^2$-s or HFU, where normal heat flow is about 1.5 HFU. To deposit 10 wt% silica over a 20-m depth range, or about 520 g silica/cm^2, requires 2000 years of such discharge, assuming the 350°C solutions precipitated 2500 ppm silica as they vented. In 2000 years at 1000 HFU, 6×10^{17} cal (2.5×10^{18} J) are vented per square kilometer. At 10^{18} cal/km^3 (Norton and Cathles, 1979), the heat required to silicify 1 km^2 of surface requires 0.6 km^3 of basaltic magma.

There could easily be ~170 km^2 of silicification at Noranda (Uzmann, 1993). *An intrusive volume of 100 km^3 would be required to produce this possible silicification.* The exposed area of the Flavrian tonnalite is ~150 km^2, however, so even if the thickness of the Flavrian were only a few kilometers, there is plenty of heat available from the intrusive. This is not intended to resolve the history of Noranda, but to illustrate the use of the equations developed above. Clearly a volume of silicified material requires a certain intrusive volume to supply enough heat. If hydrothermal silicification is extensive, a large intrusive heat source is required. The size of the intrusion can be estimated and could be of interest in mineral exploration.

FLOW FROM A SHALLOW-DIPPING AQUIFER

A similar approach can be used to analyze the steady-state temperature distribution due to outflow from a shallow-dipping aquifer system. If the aquifer segments are linear and the aquifer is thin compared to its depth, the temperature profile in each aquifer segment is determined by the temperature at a single point in that segment. If temperature at a single point in the segment is known, the temperature everywhere in the segment can be calculated. Segments may thus be joined together or daisy-chained with the temperature at the end of each segment controlling the temperature profile in the next segment. In this way, temperatures along the entire flow path can be determined by the flow rate and the temperature at just one point along the path. Since inflow temperatures will be close to ambient, temperatures can easily be calculated along any subsurface flow path in a sedimentary basin.

The daisy-chain method sketched above is fully described in Cathles (1987) and is used there to show that a Darcy flux of at least 15 m/yr in a 30-m thick aquifer is required to produce a 35°C temperature anomaly at 1-km depth when the inflow to the aquifer at 5-km depth is 300°C above the ambient surface temperature of 15°C and the dip of the aquifer is 1% (0.5°). The vertical flow rate in the aquifer is 0.15 m/yr. The thermal conductivity of the basin in this case is 3.5×10^{-3} (a low value), and the heat flow a rela-

tively high 2.1 HFU, so that the normal (unperturbed) temperature gradient in the basin is 60°C/km. Under these circumstances temperatures of 110°C are reached at 1-km depth. These temperatures and depths are appropriate for the formation of Mississippi Valley-type lead–zinc deposits. The 315°C temperature at 5-km depth is very hot for a sedimentary basin. For cooler basins greater expulsion rates would be required.

Faster expulsion rates could increase aquifer temperatures at 1-km depth to the inflow temperature at the bottom of the basin (315°C in the above example). If the flow is topographically driven, however, so that the fluids that discharge at one margin recharge at another, the maximum temperature that can be attained at 1-km depth on the discharge margin is only about half the temperature in the deepest parts of the basin. This is because the fluids entering the basin cool it substantially before they discharge.

The thermal gradient above the aquifer in this simple model is just the aquifer temperature divided by its depth. Because thermal gradient maps are available for most of the United States, methods like daisy-chaining allow thermal gradients to be inverted and aquifer flow rates to be inferred. Near-surface temperature gradients can be related very directly to fluid flow and can be used under certain circumstances to measure the rates of fluid flow in aquifers.

RATES OF SUBSURFACE FLUID FLOW

The other physical side of hydrothermal ore deposition involves the rates and mechanisms of fluid movement. Subsurface fluid flow can be driven by a variety of processes. Flow may be driven by differences in water-table elevation. Because the water table tends to follow topography, this kind of flow is often called topography-driven flow. Flow can be driven by density differences produced by temperature or salinity anomalies. This kind of flow is called thermal or haline convection. A third kind of flow is produced by the compaction that occurs when sediments accumulate in a basin or where basin sediments are overthrust. The expulsion is similar to squeezing water out of a sponge and is referred to here as compactive expulsion. Finally, flow can be produced in areas where metamorphic reactions generate fluids from minerals. Amphibolite grade devolatization reactions and the production of hydrocarbon fluids from the maturation (slow cooking) of kerogen are obvious examples, which are referred to here as metamorphic and maturation expulsion.

The flow rates produced through these mechanisms can be estimated by simple calculations. The flow of water that can be produced by each mechanism is considered in turn in the following sections. The most important basic equation governing fluid flow is Darcy's Law. It expresses conservation of momentum in a dissipative porous medium where inertial forces are unimportant. Darcy's Law can be written

$$J = -\frac{k}{\eta}(\nabla P - \rho g) \qquad (5.8)$$

where J is the Darcy flux in cm/s as before, k is the permeability of the porous medium in cm^2, η is the viscosity of the pore fluid in g/cm-s or poise, P is the pressure in dyn/cm^2, ρ is the density of the pore fluid in g/cm^3, and g is the acceleration of gravity in cm/s^2. The positive z axis points vertically upward, so $g = -g\hat{z}$.

Topography-Driven Fluid Flow

Groundwater hydrology covers topography-driven fluid flow, and many good basic references are available (De Wiest, 1965; Bear, 1972; Freeze and Cherry, 1979). Groundwater hydrologists modify Darcy's Law to consider only constant-density water. Setting $\rho = \rho_0$ = constant in equation (5.8), $-\rho g = \rho_0 g\hat{z} = \nabla(\rho_0 gz)$, so that equation (5.8) becomes

$$J = \frac{k}{\eta}\nabla(P + \rho gz) \qquad (5.9)$$

Suppose, as shown in Figure 5.1, that the elevation of the perforated part of a well casing (where pore waters are allowed in and out of the well and therefore where aquifer fluid pressure is measured) is measured in centimeters above sea level (or any other convenient elevation datum) and called the

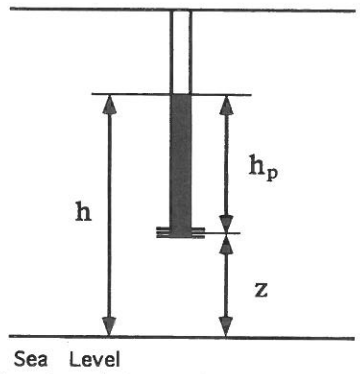

FIGURE 5.1 Schematic diagram showing the elevation, z, of perforated parts of a well relative to a reference datum such as sea level, the elevation of the water in the well relative to the observation point (perforations), h_p, and the elevation, h, relative to sea level ($h = h_p + z$).

elevation head, z. Suppose also that the static height of the water in the well is measured relative to the same datum and called the hydraulic head, h. The pressure at z equals the static standing column of water in the well and can be expressed as: $P = (h - z)\rho_0 g$. Substituting this expression for P into equation (5.9), and noting that ρ_0 and g are both constant and thus may be moved outside the gradient operator, yields the hydrogist's form of Darcy's Law:

$$J = -\frac{\rho_0 g k}{\eta} \nabla h = -K \nabla h \qquad (5.10)$$

where K is the hydraulic conductivity.

In equation (5.10) K has units of cm/s. It is common for K to be given a wide variety of different units. For example, in Figure 5.2 K has units of m/yr. From equation (5.10) hydraulic conductivity, K, and permeability, k, are related: $K[cm/s] = \rho_0 g k/\eta \approx 10^5 k[cm^2]$. A more usual unit of measure for k is the darcy, where 1 darcy = 10^{-8} cm^2. Thus $K[m/s] \approx 10^{-5} k$ [darcies].

Hydraulic conductivity can be measured in a particularly simple way that is the basis for the percolation test required for septic tanks. Hydraulic conductivity is the maximum flux (sprinkling rate) a porous medium can accommodate without ponding. As illustrated in Figure 5.1, the hydraulic head, h, in equation (5.10) is the sum of the pressure head, h_p, and the elevation head, z, so that $h = h_p + z$. If there is no ponding and the water saturation of the soil is almost, but not quite, 100%, the pressure head is zero (atmospheric) everywhere in the soil. The head is therefore exactly the elevation head. Consequently, $\nabla h = \nabla z = 1$, and, from equation (5.10), $J_z = -K$. Thus hydraulic conductivity is directly measured by the maximum rate at which water can seep into the ground without ponding.

Figure 5.2 shows that the hydraulic conductivity of naturally occurring material varies from 10^{-6} to 10^7 m/yr. Gravels could allow water to seep into the ground at a rate that would allow a column of water 10,000 km high to disappear in one year, while clays could prevent even 0.1 μm of water from seeping into the ground in one year. There is a 13 order-of-magnitude range in the permeabilities of natural materials!

Fortunately, yearly precipitation places an upper bound on topographically driven flow rates. Typically, one-third of the rainfall in an area infiltrates. Rainfalls of 10 m/yr and more occur in some rain forests but generally rainfall is less than 1 m/yr. Flow in a shallow-dipping aquifer is increased by the infiltration divided by the sine of the dip angle. For a 5° dip the infiltration is increased by an order of magnitude; for 0.5° (or 1%) dip the increase is two orders of magnitude. All considered, an approximate upper bound on Darcy flux for topographically driven flow is ~30 m/yr, but usually the Darcy flux in aquifers is ~0.1–1 m/yr, giving (for 10% porosity) true fluid velocities between 1 and 10 m/yr. The true velocity of groundwater through the J Aquifer in the Great Artesian Basin of Australia, for example, is ~1–5 m/yr (Halbermehl, 1984).

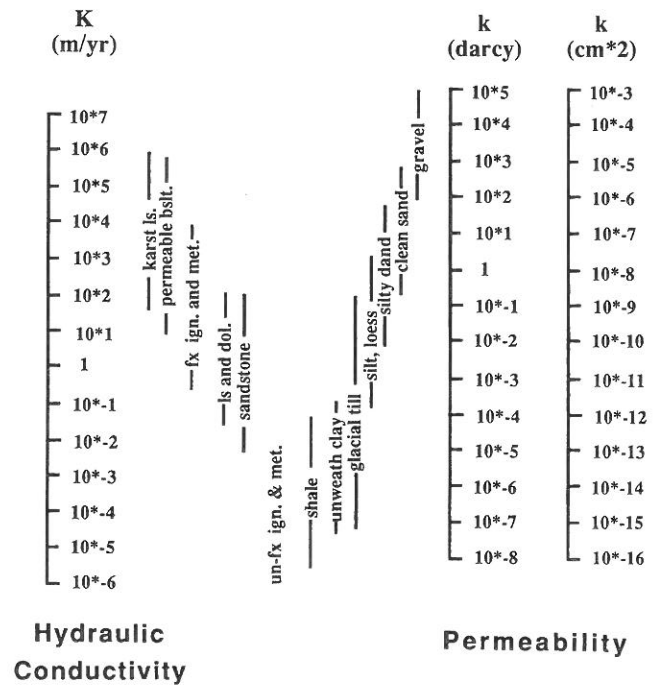

FIGURE 5.2 Hydraulic conductivities and permeabilities of common sediment and rock types (adapted from Freeze and Cherry, 1979).

Convective Flow

Convective flow is driven by differences in fluid density. As discussed in Chapter 10 of Barnes (1979), a great deal can be learned by exploring the conditions under which no flow will occur. From equation (5.9), J can be zero if the permeability is zero (not a very interesting or even realistic case) or if

$$0 = \nabla P - \rho g$$

Writing out the vector components of this equation explicitly,

$$\begin{pmatrix} \frac{\partial P}{\partial x} \\ \frac{\partial P}{\partial y} \\ \frac{\partial P}{\partial z} \end{pmatrix} = \rho \begin{pmatrix} 0 \\ 0 \\ g \end{pmatrix} \qquad (5.11)$$

shows that there will be no convective flow if fluid density is a function of z only and the vertical pressure gradient at any depth equals ρg. Flow will be produced if there are any horizontal variations in ρ, however. This is because, from the third component of equation (5.11),

$$P = -g \int_{z_s}^{z} \rho \, \partial z$$

If ρ were a function of horizontal position, P would vary horizontally and the horizontal gradients of P would be nonzero, in contradiction to the requirements that the first two components of equation (5.11) be zero. Thus a necessary condition for no flow in the subsurface is that density is a function of depth only; that is, $\rho = \rho_0(z)$.

Temperature will typically increase linearly with depth and can be characterized by a geothermal gradient, G_T[°C/cm]. With the coordinate system chosen such that the surface is at $z = 0$ and z is positive upward, G_T might typically have a value of −25°C/km or -25×10^{-5}°C/cm. If the coefficient of thermal expansion of water is α and the density of water at 0°C is ρ_{00}, then the temperature, fluid density, and pressure under no-flow conditions (indicated by the subscript 0) can be expressed as

$$T_0(z) = T_s - G_T z \qquad (5.12a)$$

$$\rho_0(z) = \rho_{00} - \rho_{00} \alpha G_T z \qquad (5.12b)$$

$$P_0(z) = -\rho_{00} g z + \frac{\rho_{00} \alpha G_T z^2}{2} \qquad (5.12c)$$

where T_s is the ambient average temperature at the surface. Note that, since G_T is negative, and z is negative downward, equation (5.12c) indicates that the pressure increases with depth at a decreasing rate. This is because increasing temperature causes increased thermal expansion and decreased fluid density. $P_0(z)$ is the cold water hydrostatic gradient.

Fluid density may develop horizontal variations and cause convective fluid circulation in the subsurface in two ways. If the thermal gradient is too large or the subsurface is permeable over a substantial depth interval, a critical Raleigh number (defined below) may be exceeded, in which case free-convection cells will develop. This convection will produce and sustain horizontal temperature gradients appropriate to drive the convection. The free fluid circulation is more vigorous the more supercritical the Raleigh number and will continue until mineral precipitation or other processes reduce the permeability and the Raleigh number falls below its critical value. There is no free convection if the Raleigh number is less than its critical value.

Convective pore-water circulation can also occur if external factors set up horizontal variations in fluid density. This is called forced convection and is the most important kind of convection for hydrothermal ore deposits. Horizontal temperature gradients and forced convection are produced along the near-vertical boundaries of an intrusive body and by horizontal variations in rock thermal conductivity. Convection is forced in the sense that it will occur at the rate allowed by the permeability regardless of whether a critical Raleigh number has been exceeded or not.

FREE CONVECTION

The Raleigh number, R, is given by the following expressions:

$$R = \frac{C\rho^2 g \alpha k H^2 G_T}{\eta K} \qquad (5.13)$$

where H is the thickness of the lithologic layer and the other parameters are as defined previously. The critical Raleigh number depends on whether free flow is allowed out the top surface of the layer. If free flow is allowed, $R_C = 27$ and if free flow is not allowed $R_C = 4\pi^2$ (Lapwood, 1948). For G_T = 25°C/km and H = 5 km, the free-flow critical Raleigh number is exceeded if $k > 0.3$ millidarcy (0.3×10^{-11} cm^2). This is a reasonable permeability for the subsurface, as indicated by measurements in the Gallapagos area (Fehn et al., 1983), and therefore free convection could be an important geological process. It could cause significant subsurface redistribution of silica. Salinity stratification (Frape and Fritz, 1987) probably eliminates free convection in most old terrains, however.

The maximum vertical flow rate for the no-outflow boundary condition is proportional to the square root of the difference between the Raleigh number and the critical Raleigh number (Donaldson, 1962; Combarnous and Bories, 1975):

$$J_z = \frac{\sqrt{2}\,K}{\rho c H} (R - R_c)^{0.5} \qquad (5.14)$$

For $K = 4 \times 10^{-3}$ cal/cm-s-°C, H = 5 km, $\rho C = 1$, $R = 50$, and $R_C = 4\pi^2$, $J_z = 0.012$ m/yr. For $R = 100$, $J_z = 0.028$ m/yr.

FORCED CONVECTION NEAR AN INTRUSION OR SALT DOME

Forced convection is of particular interest to hydrothermal ore deposits because it can be much more vigorous than free convection and therefore can sustain high temperatures and steep temperature gradients near the surface. Estimates of the magnitude of forced convective flow are made most easily if flow is considered to result from a perturbation pressure, P_1, an anomalous fluid density, ρ_1, and an anomalous temperature, T_1, defined:

$$P(\mathbf{x}, t) = P_0(z) + P_1(\mathbf{x}, t) \qquad (5.15a)$$

$$\rho(\mathbf{x}, t) = \rho_0(z) + \rho_1(\mathbf{x}, t) \qquad (5.15b)$$

$$T_1(\mathbf{x}, t) = T_0(z) + T_1(\mathbf{x}, t) \qquad (5.15c)$$

Since from equation (5.11) no fluid flow requires $\nabla P_0 - \rho_0 \mathbf{g} = 0$, substitution of equation (5.15b) into (5.8) yields a new form of Darcy's Law:

$$J = -\frac{k}{\eta}(\nabla P_1 - \rho_1 \mathbf{g}) \qquad (5.16)$$

It can be seen explicitly from equation (5.16) that flow in the subsurface is driven by pressure and fluid density perturbations relative to the normal or zero-order (no flow) values of these variables that are given in equations
(5.12a,b,c).

Convective inflow near an intrusive body will not perturb subsurface fluid pressures very much, because the inflow will be over a large area and slow. If there is no barrier between areas of cold water inflow and hot fluid upflow near an intrusive, cold water hydrostatic pressures will impose themselves on the upflow zone (Elder, 1966). They will squeeze and narrow it until the rate of upflow compensates for the lower density of the hot fluids and the pressure gradient in the upwelling areas matches the cold water hydrostatic gradient. Mathematically, this means that in equation (5.16) the upflow zone $\nabla P_1 = 0$. The rate of upflow is thus

$$J = \frac{k}{\eta}\rho_1 \mathbf{g} \qquad (5.17)$$

Since $\mathbf{g} = -g\hat{\mathbf{z}}$, and $\rho_1 = -\rho_{00}\alpha T_1$, the rate of thermally forced convective flow at the margin of an intrusive is

$$J = \frac{k\rho_{00} g \alpha T_1}{\eta}\hat{\mathbf{z}} \qquad (5.18)$$

For $\alpha = 10^3/°C$, $g = 10^3$ cm/s^2, k = 1 millidarcy = 10^{-11} cm^2, $\eta = 0.002$ g/cm-s, and $T_1 = 300°C$, J = 0.47 m/yr. The upflow rate near an intrusion margin

is thus about

$$J = 0.47k[md]\ m/yr$$

If the permeability were 10 millidarcies (md), for example, the vertical Darcy flux would be 4.7 m/yr; if T_1 were 150°C rather than 300°C the flow rate would be halved.

Rates of haline convection can be estimated in the same way. The perturbation in density is due to salinity rather than temperature. If salinity, C, is measured as the mass fraction salt, $\rho_1 \approx \rho_{00}C$, and cases of haline convection near the margin of a salt dome can immediately be estimated from equation (5.17). For the same parameters as before and 1-millidarcy permeability, the downflow near a salt dome that causes adjacent fluids to be 22 wt % more saline than adjacent regional fluids would be ~0.34 m/yr. The flow rate is a little less than the thermal upflow rate in the previous example because the perturbation of density caused by increasing temperature by 300°C is 0.3 g/cm^3, whereas the increase in density due to salt addition is ~0.22 g/cm^3.

FORCED CONVECTION IN SEDIMENTARY STRATA

Another example of forced convection that is indirectly of considerable economic interest is the forced convection that occurs when lithologic strata of differing thermal conductivity are folded. If sedimentary strata with differing thermal conductivities are deformed such that their contact is no longer horizontal, horizontal temperature gradients are established and these gradients drive forced convection.

The magnitude of the forced convection can be estimated in a fashion identical to that used in the preceding section. Consider a sand layer enclosed by shale (Figure 5.3). If a sand layer, of thickness Δh and thermal conductivity K_s, is dipping at a small angle with slope S, the regional heat flow, J_H, is uniform, and the thermal conductivity of the shale is K, the difference in temperature horizontally across a sand layer, ΔT, as illustrated in Figure 5.3 is

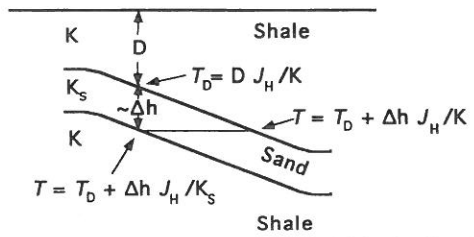

FIGURE 5.3 Temperatures at the same elevation on either side of a shale-hosted sand layer of thickness Δh.

$$\Delta T = \left(D\frac{J_H}{K} + \Delta h\frac{J_H}{K}\right) - \left(D\frac{J_H}{K} + \Delta h\frac{J_H}{K_s}\right)$$

$$= \frac{\Delta h J_H}{K_s}\left(\frac{K_s}{K} - 1\right) \qquad (5.19)$$

If the thermal conductivity of the sand is greater than the shale that encloses it, the temperature at the top of the sand layer will be $\Delta T/2$ greater than at the same depth in the middle of the layer, and the temperature at the bottom of the layer will be $-\Delta T/2$ less than that in the middle of the layer at the same depth. Water at the top of the layer will circulate upward, fluid at the base downward, and fluid in the center of the layer will be static. The zero-order (stagnant) hydrostat can therefore be conveniently defined by the temperatures and fluid densities in the middle of the layer. The Darcy flux along the top of the sand layer, $J_{\|+}$, then follows immediately from equation (5.18):

$$J_{\|+} = \frac{k}{\eta}\left(\rho_{00}\alpha\frac{\Delta T}{2}\right)(g_0 S) \qquad (5.20)$$

where ΔT is given by equation (5.19). Note that only the component of g_0 parallel to the sides of the sand layer is effective in driving flow and therefore g_0 has been modified to $g_0 S$, where S is the slope of the layer.

If the sand layer is sinusoidally folded with amplitude a and wavelength λ, and S is taken to be the maximum slope of the layer at $x = \lambda/2$ so that $S = 2\pi a/\lambda$, equation (5.20) yields

$$J_{\|+} = \frac{k}{\eta}\left(\rho_{00}\alpha\frac{1}{2}\frac{\Delta h J_H}{K_s}\left(\frac{K_s}{K} - 1\right)\right)\left(g_0\frac{2\pi a}{\lambda}\right) \qquad (5.21)$$

This is identical to the exact solution for a simple folded layer surrounded by shale (Davis et al., 1985). The vertical fluid velocity is $J_{\|+}S = J_{\|+}(2\pi a/\lambda)$. Taking $J_H = 1.2 \times 10^{-6}$ cal/cm^2-s, $\Delta h = 100$ m, $K = 3 \times 10^{-3}$ cal/cm-s-°C, $K_s = 5 \times 10^{-3}$ cal/cm-s-°C, $\lambda = 10$ km, $a = 100$ m, $k = 10$ darcies $= 10^{-7}$cm^2, and the other parameters are as in the previous calculations, $J_{\|+} = 0.8$ m/yr and $J_z = 0.05$ m/yr, values close to those estimated by Wood and Hewett (1982). Thus substantial forced circulation can occur in thick, permeable, nonhorizontal, shale-hosted sand bodies just as a consequence of contrasting thermal conductivity.

Because convection can persist for very long periods of time, substantial redistribution of silica may result (Wood and Hewett, 1982). For example, following Wood and Hewett and taking a typical temperature dependence of silica solubility of 5 ppm SiO_2/°C, a vertical upflow of 5 cm/yr will deposit 2.3×10^{-9} cm^3 SiO_2/yr[$= (5\times10^{-6}$g SiO_2/g $H_2O)(\rho_{H_2O}/\rho_{SiO_2})G_T V_z$], and 10 vol % silica can be deposited in 43 million years [$= (0.1$ cm^3 SiO_2/cm^3)/(2.5×10^{-9} cm^3 SiO_2/cm^3-hr)].

FORCED CONVECTION IN A RADIOGENIC INTRUSION

Finally, radiogenic heat can steadily maintain horizontal temperature gradients and drive forced convection. Fehn et al. (1983) showed that if the permeability was very low so that there was no convection, an intrusion having the size and radioactivity of the Conway, New Hampshire Granite would steadily maintain its center at 10-km depth at temperatures ~140°C hotter than those at the same depth far from the intrusion. If the granite and its surroundings had 0.1-millidarcy permeability, the Darcy flux through the intrusion would be a few centimeters per year, and a mass of water equal to that of the Conway Granite could be circulated through it in less than 10 million years. Fehn et al. suggested that such radiogenic thermal circulation could account for vein uranium deposits associated with radiogenic intrusions. Whenever a radiogenic granite is fractured, circulation may remobilize uranium into the fracture system. Long-lived radiogenic convection may also have produced the china clays in Cornwall (U. Fehn, personal communication, 1983).

Expulsive Flow

Fluids can be expelled from a basin by compaction or as the result of reactions that convert solids to lower density fluids. The expulsion rate can be estimated by equations expressing conservation of solid and fluid mass.

Conservation of solid mass for uniform sediments requires that the same solid mass pass all depth horizons as the basin subsides. If $v_s(z)$ indicates the subsidence rate (relative to the basin surface), this means that

$$v_s(z)[1 - \phi(z)] = \text{constant}$$

Application to both the surface and depth z shows that the subsidence at depth z is a function of the surface sedimentation rate S, the deposition porosity ϕ_0, and the porosity at z, $\phi(z)$:

$$v_s(z) = S\frac{1 - \phi_0}{1 - \phi(z)} \qquad (5.22)$$

COMPACTIVE EXPULSION

Conservation of pore-fluid mass requires that the compactive efflux of pore fluids at a depth z, $J_c(z)$, equal the difference between the water carried in at z and out at the base of the basin, z = b:

$$J_c(z) = v_s(z)\phi(z) - v_s(b)\phi(b)$$

If the basement is considered impermeable and there is no horizontal flow (as is assumed here), the expulsive Darcy flux will be vertically upward. The direction of flow (sign of J_c) is provided by geological considerations. From equation (5.22),

$$J_c(z) = \left(\phi(z) - \phi(b)\,\frac{1-\phi(z)}{1-\phi(b)}\right) v_z \qquad (5.23)$$

A "typical" compaction curve (Hanor, 1979) is

$$\phi(z) = 0.7\exp(0.57z[\text{km}]) \qquad (5.24)$$

where z is measured in kilometers and is negative downward into the basin from z = 0 at the basin surface. Taking b = −8 km and z = −3, we find

$$\begin{aligned} \phi(z=0) &= 0.70 = \phi_0 \\ \phi(z=-3\text{ km}) &= 0.13 \\ \phi(z=-8\text{ km}) &= 0.007 \\ J_c(z=-3\text{ km}) &= 0.12v_z \\ v_z(z=-3\text{ km}) &= 0.34S \\ J_c(z=-3\text{ km}) &= 0.04S \end{aligned} \qquad (5.25)$$

For S = 0.1 to 1 km/Ma,

$$J_C(z=-3\text{ km}) = 4\times10^{-5}\text{ to }4\times10^{-6}\text{ m/yr}$$

Compactive fluid expulsion rates from sedimentary basins are about four orders of magnitude smaller than the topographic and convective Darcy flux rates we have previously been considering.

AQUATHERMAL EXPULSION

Pore fluids are also expelled from a basin as the pore fluids are buried, heated, and thermally expand. For uniform burial rates the rate of heating is approximately constant and can be characterized by H_r. For example, in a basin accumulating sediments at 1 km/Ma, H_r would be about 25°C/Ma if the geothermal gradient in the basin, G_T, were ~25°C/km. If the coefficient of thermal expansion of the pore fluid is α, the increase in pore fluid volume at any depth is $\phi(z)\alpha H_r$, and the total rate of expansion between z and b, and therefore the total aquathermal expulsion, J_{at}, is

$$J_{at}(z) = \int_z^b \phi(z)\alpha H_r\,dz$$

If we approximate $H_r = v_z(z=-3\text{ km})G_T$, integration together with equation (5.24) yields

$$J_{at}(z=-3\text{ km}) = \frac{\phi(z=-3\text{ km}) - \phi(b)}{0.57}\,\alpha G_T v_z(z=-3\text{ km}) \qquad (5.26)$$

For $\alpha = 10^{-3}$/°C and a thermal gradient G_T = 25°C/km, and b = 8 km as before, equation (5.26) gives

$$J_{at}(z=-3\text{ km}) = 0.005v_z$$

Aquathermal expulsion is about 4% of compactive expulsion.

MATURATION EXPULSION

The vertical flux of fluids from chemical reactions in a sedimentary basin is easily estimated if those reactions begin below z and go to completion above the basement, z = b. If the grade of the reacting material is c_i grams of i per gram of solids, ρ_s is the density of the solids, and ΔV_i is the change in volume upon complete reaction of i, the upper bound on the fluid flux, J_i, due to reaction i is

$$J_i < \Delta V\, c_i \rho_s v_z \qquad (5.27)$$

The efflux will be less than indicated by equation (5.27) because the reaction goes to completion below z, where the subsidence rate is less than v_z.

Kerogen matures progressively to gas in the deep portions of sedimentary basins (see Chapter 12). The deeper methane-generating reactions that generally occur below a 3-km depth are dominated by the conversion of earlier-generated oil to methane. For type II (marine) kerogen about 0.4 g of oil with density 0.8 g/cm^3 are generated per gram of original kerogen, and the oil decomposes to 0.24 g CH_4 with density ~0.16 g/cm^3 and 0.16 g of residua with density 2 g/cm^3 (J. Hunt, personal communication, 1989). The density of methane given here was calculated for 87°C and 290 bars using the Behar (Behar et al., 1985) equation of state. These pressures and temperatures are typical of conditions at a 3-km depth in hydrostatically pressured sediments above the overpressured zones that typically lie below this depth in actively infilling basins. The volume change of the oil decomposition reaction is 1.1 cm^3/g kerogen. Thus if $c_K\rho_s = 0.1$, from equation (5.25)

$$J_{CH_4} = 0.11v_z \qquad (5.28)$$

Comparing equation (5.28) with (5.25) shows that the efflux of pore fluids due to the maturation of reasonably organic-rich sediments in a basin is comparable to the efflux that could be caused by compaction! The burial of organic-rich sediments into the gas generation window can be as effective in generating overpressures and expelling pore fluids as compaction, a

possibility of considerable interest to the formation of Mississippi Valley-type (MVT) deposits. It was suggested as a fluid expulsion mechanism for the classic midcontinent of the United States by Rich (1927) and has interesting implications for coupling fluid expulsion and the formation of MVT lead–zinc deposits to sea level regressions (Eisenlohr et al., 1994).

METAMORPHIC EXPULSION

Amphibolite grade metamorphic reactions liberate water bound in hydrous minerals. Likely rates of metamorphic fluid expulsion can be estimated in a fashion similar to that discussed above if v_z is considered the migration rate of a thermal front away from an intrusive body rather than the subsidence rate at z. This is because, in equation (5.24), v_z is really an estimate of the rate at which the thermal gradient moves through sediments in the basin. For example, far enough up in the sedimentary sequence, temperatures are cool enough that the reaction in question has not occurred. Deep enough into the basin, temperatures are hot enough that the reaction is fully completed. Because the geothermal gradient in a basin is not affected greatly by the sedimentation rates considered here, the subsidence velocity, v_z, is the rate at which sediments move across the maturation boundary.

We need a way to estimate how rapidly the intrusive will heat its surroundings. A conductive thermal front migrates a distance $z = 2\sqrt{\kappa t}$ away from the hot surface of an intrusion in time t (Carslaw and Jaeger, 1959). Taking the derivative of this expression, we see that the rate of migration of the temperature isotherms is proportional to the thermal diffusivity of the rock and inversely proportional to time

$$v_z = \sqrt{\frac{\kappa}{t}} \qquad (5.29)$$

For $\kappa = 0.01$ cm^2/s,

$$v_z[\text{km/Ma}] = \frac{5.6}{\sqrt{t[\text{Ma}]}}$$

$$= 5.6\text{–}177 \text{ km/Ma for } t = 10^6 \text{ to } 10^3 \text{ yr}$$

This calculation presumes that metamorphism is driven by igneous intrusion or delamination of the lithosphere. Evidence of fluid flow and high-T, low-P metamorphism during deformation suggests this geologic concept (Etheridge et al., 1987; Loosveld and Etheridge, 1990; Sandiford and Powell, 1991). Metamorphism by overthrusting produces slower rates of fluid expulsion, as will be briefly reviewed below.

It can be seen from equation (5.29) that the migration rate of a thermal front, although very rapid immediately following intrusion, drops to <200 km/Ma after 1000 years. The most relevant time interval is between ~10^3 and ~10^6 years because over this interval of time temperatures migrate outward from ~0.35 to ~11 km and this is therefore the interval of time during which most of the rock volume is metamorphosed.

Because metamorphic reactions liberate ~1 wt % CO_2 and ~3 wt % water (Phillips et al., 1987; Labotka, 1991) without much density change of the hydrous minerals, taking a fluid density of 1 yields a volume change of 0.1 cm^3/cm^3 [which equates to $\Delta V c_i \rho_s$ in equation (5.27)]. Considering the case where sills are emplaced under extensive areas and heat the overlying cover by upward conduction, equation (5.29) indicates that the metamorphic fluid expulsion rates will typically be

$$J_{met} \approx 0.1 v_z \qquad (5.30)$$

This is about the same as the compaction and maturation expulsion rates estimated in equations (5.25) and (5.27). However, the conductive migration of thermal fronts is much faster than the sediment subsidence rate in sedimentary basins. For v_z = 200 km/Ma, equation (5.30) indicates that $J_{met} \approx 0.02$ m/yr, a value in general agreement with other estimates (Furlong et al., 1991; Hanson, 1992).

Under the other common metamorphic model (sudden overthrusting and doubling of the crustal thickness followed by erosion), the expulsion rates are much smaller. In this case, Connolly and Thompson (1989) have shown that metamorphic fluids will be expelled at up to 6×10^{-5} m/yr, about the same rate as they are expelled in the most actively infilling sedimentary basins by compaction or gas generation.

Summary

The estimates of subsurface fluid fluxes made above are, of course, approximate. Nevertheless, broad magnitude generalizations can be drawn as illustrated in Table 5.1. Compactive expulsion of pore fluids or the expulsion of hydrocarbons generated in sedimentary basins is the slowest major flow process considered and drives average vertical pore fluid fluxes of <0.0000X m/yr, where X is a number such as 4. Rates of metamorphic fluid expulsion in greenstone belts can be several orders of magnitude higher and are similar in magnitude to the rates of free convection and convection forced by thermal conductivity variations in folded sand layers. Forced convection rates depend on permeability and therefore span a wide range of magnitudes. Recent analyses summarized in the next section suggest that they can be very rapid and many orders of magnitude greater than topographically driven fluxes.

TABLE 5.1 Upper Bounds on Water Discharge Fluxes from Flow Systems Considered in the Text

XOOOO	m/yr	Megaplume discharge rates
XOO	m/yr	Upflow near igneous intrusion
X	m/yr	Topographically driven flow
0.X	m/yr	Haline convection near salt domes
0.0X	m/yr	Free convection, convection in folded sand layers; metamorphic expulsion
0.0000X	m/yr	Compactive or maturation expulsion in sedimentary basins (1 km/Ma sedimentation rate), or metamorphism in overthrust
0.00000X	m/yr	Aquathermal expulsion in sedimentary basins (1 km/Ma sedimentation rate)

FLUID FLUXES, TEMPERATURE, AND ORE DEPOSITION

The methods for estimating the rates and thermal consequences of subsurface fluid flow can now be applied to observations in active and fossil hydrothermal systems to better understand how these systems work and to more clearly assess how to explore for them. From a fluid flow perspective, hydrothermal ore deposits fall into three main categories: (1) those produced by precipitation from topographically driven fluids (e.g., roll-front uranium deposits and perhaps MVT lead–zinc deposits), (2) those precipitated from convectively circulated fluids (e.g., volcanogenic massive sulfide deposits and many vein deposits), and (3) those precipitated from compactively or chemically expelled fluids (e.g., porphyry copper deposits, probably MVT lead–zinc deposits, and probably greenstone gold deposits). In this final section analysis techniques are illustrated by application to the last two kinds of deposit.

Convective Deposits

INTRUSIVE COOLING TIME

One of the most fundamental and important questions is: How long will it take an intrusion to cool if it interacts with convecting pore waters? A related question is: At what permeabilities does convection start to become important in speeding the cooling of an intrusion? These questions can be answered in an approximate but useful manner if it is assumed that the intrusion has the same permeability as its host environment and that it is therefore simply a volume initially T_1^o degrees Celsius hotter than its surroundings. T_1 is

defined by equation (5.15) and the superscript "o" indicates that it is the original temperature contrast.

If the hot zone is of height H and uniform sectional area, and the Darcy flux is uniform throughout the rock prism, then, ignoring heat sources and conductive heat losses, equation (5.1) may be integrated from the base to the top of the hot zone:

$$\rho_m C_m H \frac{\partial T_1}{\partial t} = -J \rho C T_1 \qquad (5.31)$$

Replacing J with (5.18), rearranging so that T_1 is on the left and t on the right, and integrating from $t = 0$ to t and $T_1 = T_1^o$ to T_1, yields

$$t = t_c \left(\frac{T_1^o}{T_1} - 1 \right), \quad \text{where} \quad t_c = \frac{\eta \rho_m C_m H}{k \rho^2 C \alpha g T_1^o} \qquad (5.32)$$

Equation (5.32) shows that the time to convectively cool an intrusion to 25% of its initial temperature constrast is $3t_c$. For H = 3 km, k = 1 millidarcy, T_1^o = 600°C, and the other parameters as specified previously, this cooling will require 3900 years. The time to cool increases as the height of the intrusion increases, and decreases with increasing permeability and T_1^o.

Equation (5.32) was used in Cathles (1981) to construct the diagram reproduced here as Figure 5.4, which shows how an intrusion with a specific geometry will cool by conduction or convection. If cooling is by conduction, the time to cool to 25% of the initial temperature contrast will increase as the dimension of the intrusion squared (Carslaw and Jaeger, 1959). These cooling times shown on the ordinate are plotted against the halfwidth, a, of the intrusion on the abscissa. The time to cool a dike that extends from the surface to infinite depths (called an infinite dike) is slightly longer, as illustrated by the parallel dashed line just to the left of the first solid line. The time to conductively cool the dike if its sides are initially set and subsequently retained at $T_1 = 0$ is shown as the parallel dot-dashed line with slope of 2 to the right of the first solid line. This line illustrates that an impermeable dike emplaced in a very permeable environment, in which pore water convection maintains its sides at ambient temperatures, will cool more rapidly, but that the cooling times will still have the characteristic conductive dependence on a^2 (slope of 2 on this log–log plot). The diagram is capped by the cooling times at 5-km depth of an infinite sill of thickness 6a whose top is at the surface. The cooling time at 5-km depth within this sill is not increased after the sill reaches a thickness of ~40 km. This is the maximum time that a point at 5-km depth could possibly take to cool to 25% of T_1^o.

Within this conductive context, lines with slope of 1 illustrate the times required to cool an intrusion by convection. The lines are drawn strictly on the basis of equation (5.32) but have been confirmed by numerical calculation

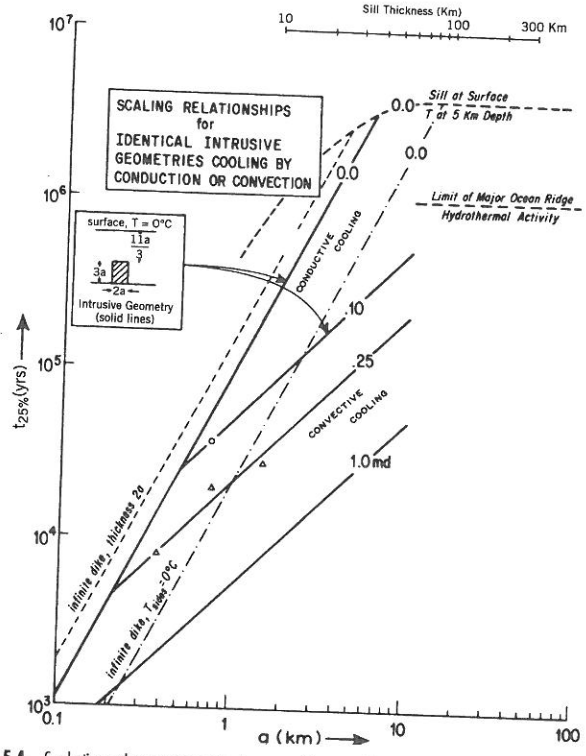

FIGURE 5.4 Conductive and convective cooling times as a function of the halfwidth, *a*, of the intrusion shown in the insert. [Reproduced with permission from the 75th Anniversary Volume of *Economic Geology* (1981, p. 439).]

[circles and triangles along lines as discussed in Cathles (1981)]. The intersections of the convective and conductive lines indicate the permeabilities at which convection will speed the rate of cooling. For example, a permeability of 0.25 millidarcy will accelerate the cooling of intrusions wider than about 400 m in a permeable zone 1.33 km deep.

Figure 5.4 shows that there is a sharp permeability cutoff between conductive and convective cooling. For example, from Figure 5.4 it is apparent that a 2-km wide intrusion will cool by conduction provided that the permeability is ≤0.055 millidarcy. The time it takes to cool to 25% of T_1° is about 10^5 years. However, if the permeability is only ~4 times greater (0.25 md) the cooling is dominantly by convection and the cooling takes place in

~25,000 years. A factor of 4 is a very small permeability increase given the huge range of permeability variations in nature (see Figure 5.2), and thus intrusions will tend to either cool entirely by conduction or by convection and not by a combination of conduction and convection.

A second important conclusion indicated by Figure 5.4 is that cooling times of even quite large intrusions will be short (less than 10,000 years) if the subsurface permeability approaches 1 millidarcy. Such permeabilities are probably common in the subsurface. Where permeabilities are of this order, intrusions will be cooled rapidly by convecting pore waters. Discharging hydrothermal waters will produce geothermal systems and perhaps ore deposits because the flow rates will be rapid enough to carry hot water to the surface. The existence of hydrothermal systems and ore deposits indicates that subsurface permeabilities are sufficient to make convective cooling the dominant cooling mechanism.

TEMPERATURE DEPENDENCE OF PERMEABILITY

Although very useful and valid in a general sense, the assumption underlying Figure 5.4 that rocks at >600°C are as permeable as their host is clearly wrong. There is certainly a dependence of permeability on temperature. At some temperature rocks will become plastic enough that the fractures through which flow takes place will heal and the rocks will become impermeable. Observations of typical venting temperatures in forced thermal convection systems and computer simulations that incorporate the thermodynamic properties of water indicate that the permeability cutoff occurs at $T \approx 350$°C (Cathles, 1983).

All convective systems seem to have maximum fluid temperatures of ~350°C. Black smoker venting on the seafloor is at this temperature, as are the deep, preboiling fluids in continental geothermal systems. Maximum temperatures in volcanogenic massive sulfide deposits and hydrostatically pressured vein deposits are inferred from mineralogical, isotopic, and fluid inclusion data to be in this range. The frequency with which fluids of 300–350°C are encountered in active and fossil hydrothermal systems is a well documented (Polster and Barnes, 1993) observation that must be explained.

It has been suggested that the fluid temperature is related to the triple point of water. Bischoff and Rosenbauer (1985), for example, argued that convection downward toward a hot surface will turn upward when low densities near the critical point are reached. This scenario is possible for a carefully contrived case of uniform heating from an absolutely flat hot pad (free convection), but hydrodynamic calculations show that the Bischoff–Rosenbauer mechanism will not work in the more common case of forced convection, where, for example, the exposed margin of an intrusive heats adjacent pore waters and causes them to convect upward. Calculations show that in this situation the thermodynamic properties of water make the upward transport of heat more rather than less efficient and cause the fluids that exit the surface to

reflect more rather than less closely the temperature at which they are able to interact with the rock (Cathles, 1983). In this case, the thermodynamic properties of water are completely ineffective in controlling water temperature. The only control on the preboiling discharge temperature during forced thermal convection appears therefore to be the temperature at which most of the circulating water flows through the rock. If hydrothermal fluids are to be ≲350°C, permeability must be a function of temperature such that it is much smaller above 300–350°C.

This dependence of permeability on temperature does not mean that water cannot interact with rock at higher temperatures. Some interaction can and does take place as discussed in the next section. The dependence of permeability on temperature simply means that most of the pore water circulates through rock at $T \lesssim 350$°C. The permeability reduction appears to be related to pressure-driven rates of dissolution, where opposite sides of a fracture make contact. When temperatures of about 350°C are reached, the rate of dissolution at these locations is rapid enough to heal the fracture between rupture events. All other factors being equal, tectonically active areas may typically have slightly higher hydrothermal system temperatures than tectonically inactive sites. The difference in flow temperature is not expected to be large, however, because the rate of the dissolution reactions doubles for every ~10°C increase in temperature. Therefore a site 10 times more tectonically active would be expected to operate at only ~35°C higher temperature.

The idea that there is a strong temperature effect on permeability that is effective above ~350°C has many implications. For example, this hypothesis suggests that hydrothermal systems that operate at significantly different temperatures, such as hotter porphyry copper and cooler MVT lead–zinc systems, involve a nonconvective flow mechanism. It suggests that thermodynamic parameters at $T \lesssim 350$°C will suffice to characterize much of the alteration. It suggests that 350°C venting will operate as long as partially molten crystalline mush remains for a thermal cracking front to attack, and will cease as soon as this is not the case. Temperatures in a hydrothermal system will drop very rapidly as soon as there are no more magmas to buffer the heat supply (see next section). Black smoker venting thus requires the presence of magma.

The 350°C cutoff suggests hydrostatic conditions may persist in the Earth's crust to about the 350°C isotherm, and that therefore topography- or convection-driven flow may occur to depths of ~15 km but not at greater depths were fractures will be closed and impermeable. Because the rocks are so impermeable below 15 km depth and above 350°C, pore fluids in these environments will tend to be overpressured. This basic permeability and pressure division may explain Archean lode gold deposits. These deposits are thought to form by fluid decompression at the amphibolite–greenschist boundary when fluids decompress from lithostatic to hydrostatic pressures. A temperature-dependent (350°C) pressure and permeability division is also compatible with the general assumption in metamorphic petrology that metamorphic reactions at amphibolite or higher grade occur at lithostatic fluid pressures.

MIDOCEAN RIDGE HYDROTHERMAL SYSTEMS

Four observed characteristics of midocean ridge hydrothermal systems allow four principal unknowns of the hydrothermal system to be determined by the algebraic solution of four equations. The four observations are as follows:

1. Black smoker fields commonly discharge at a total rate $Q_w \approx 75$ kg/s (Cann and Strens, 1989).
2. The discharge temperature, T_{vent}, is ~350°C.
3. The residence time, t_{fz}, of the fluids in the flow zone, from when they are heated to 150°C and anhydrite precipitates to when they vent, is <10 years (Kadko and Moore, 1988).
4. Black smoker fields can discharge at much more rapid rates for short periods of time and then return to normal rates of discharge, always at 350°C. A rapid discharge or megaplume event on the Cleft segment of the Juan de Fuca Ridge in August of 1987 discharged a volume of 350°C water sufficient to carry off 2.88×10^{16} calories (Baker et al., 1989).

Midocean ridge intrusions are generally small and their surface area (= hP, where h is the height of the intrusion above the moho and P is its perimeter as shown in Figure 5.5) can be considered reasonably well known. It is assumed here that h = 5 km and P = 12.5 km so that hP = 62.5 km. In this representative case, the principal flow parameters of the hydrothermal system illustrated in Figure 5.5 are as follows:

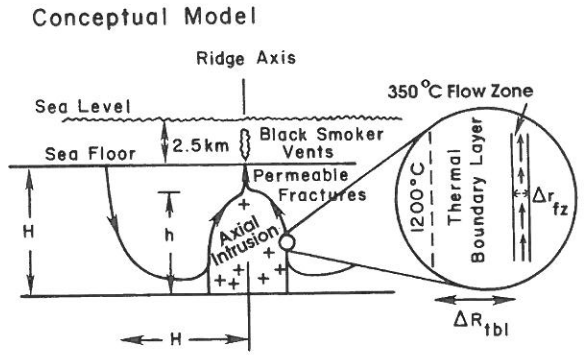

FIGURE 5.5 Geometry of the midocean ridge intrusion used in the calculations discussed in the text. [Reproduced with permission from *Economic Geology* (1993, Figure 1, p. 1979).]

1. The thickness of the 350°C flow zone along the margin of the intrusion, Δr_{fz}.
2. The permeability of the flow zone, k_{fz}.
3. The porosity of the flow zone, ϕ_{fz}.
4. The thickness of the thermal boundary layer that separates the flow zone from 1200°C parts of the intrusion, ΔR_{tbl}.

The observed variables and the unknowns are related by four equations:

$$t_{fz} = \phi_{fz} h / J_{fz} \qquad (5.33a)$$

$$Q_w = \Delta r_{fz} P \rho J_{fz} \qquad (5.33b)$$

$$Q_w T_{vent} C = J_{tbl} Ph = (K_m(1200°C - 350°C)/\Delta R_{tbl})Ph \qquad (5.33c)$$

$$Q_H = (T_{vent} - T_{amb}) C_m \rho_m \Delta r_{fz} Ph \qquad (5.33d)$$

The first equation (5.33a) states that the residence time in the flow zone equals the height of the flow zone divided by the true velocity of the fluid. The fluids are assumed to move very rapidly through the fractures above the intrusion, and therefore the transit time there is negligible. J_{fz} is the Darcy flux in the flow zone and is given by equation (5.18) with $T_1 \approx 300°C$.

In equation (5.33b) the total discharge of the black smoker field is equated to the product of the mass flux (= Darcy flux times fluid density) through the flow zone and its cross-sectional area ($P \Delta r_{fz}$).

In equation (5.33c) the normal thermal discharge is set equal to the heat steadily conducted across the thermal boundary layer.

The last equation (5.33d) states that the thermal energy discharged in a megaplume event equals the heat content of the 350°C flow zone. The concept embodied by this equation is that a tectonic event or slight magma withdrawal from the intrusion can greatly increase the permeability of the flow zone and cause its thickness to contract greatly. Permeability increases as the fourth power of effective porosity (open space through which water flows). Magma withdrawal that leads to a small increase in open space can therefore greatly increase permeability. When the permeability of the flow zone is thus increased, cold water hydrostatic pressure adjacent to the flow zone will cause the hot flow zone to contract in thickness. The heat discharged by the megaplume event is a direct measure of the change of heat content of the flow zone due to this contraction. Once the megaplume has discharged, the black smoker field will return to its earlier state of operation. The main difference between pre- and post-megaplume discharge is that the residence time of pore waters in the flow zone is greatly reduced after the megaplume event.

The four equations (5.33a–d) can be solved with the following results (Cathles, 1993a):

$$\Delta r_{fz} = 3.4 \text{ m}$$
$$k_{fz} = 350 \text{ millidarcies during normal discharge}$$
$$\phi_{fz} = 10$$
$$\Delta R_{tbl} = 180 \text{ m}$$

These values are reasonable and potentially testable by drilling. The narrow nature of the flow zone is particularly interesting because it agrees with field observations and makes the physical system vulnerable to rapid chemical changes of the kind that have been observed both on the seafloor and in fossil massive sulfide systems. In particular, as discussed in Cathles (1993a), episodic migration of the cracking front into the thermal boundary layer can produce, with such a narrow flow zone, the fluctuations of discharge salinity from half to twice seawater salinity that are observed in both fossil and midocean ridge hydrothermal systems. Additional discussion of midocean ridge hydrothermal systems can be found in Morton and Sleep (1985), Brikowski and Norton (1987), and Cathles (1993a).

Expulsive Deposits

VENTING STYLE AND ALTERATION

Both the venting style and the different effects of permeability variations make the patterns of alteration and their exploration implications quite different for deposits that are the product of compactive compared to convective flow. Cold water hydrostatic pressures compress and focus thermal convective upflow and alteration gradients can be useful in exploring for deposits formed by thermal convection. In contrast, computer simulations (Cathles and Smith, 1983) as well as logic indicate that fluids with close to lithostatic pressures escape, especially near the surface, through every available flow path. Mineral deposition from high-pressure fluids may be concentrated along major escape channels surrounded by more intense alteration, but even minor escape paths may have some mineralization and alteration. There may be regional alteration trends such as the regular lead-isotope zonation observed across MVT districts (Heyl et al., 1966), which is presumably related to progressive interaction between the escaping fluids and basement. But locally, alteration and mineralization are almost ubiquitous (Coveny et al., 1987) and difficult to use in exploration.

In addition, as discussed earlier, thick sand lenses in sedimentary basins may permit fluids to circulate internally and, over a relatively short time (a few tens of millions of years), cause significant silicification and alteration. Such alteration has nothing to do with the pore-water throughflow that forms hydrothermal ore deposits. It must be distinguished from the flow responsible for mineralization if alteration is to be used to guide exploration.

THERMAL PERTURBATIONS AND THEIR IMPLICATIONS

Many basin-hosted deposits were thermal anomalies at the time of ore deposition. Generating fluid fluxes large enough to produce these thermal perturbations is a major constraint on genetic hypotheses. The calculations presented in the previous section show that under the most favorable circumstances (a sudden intrusion or underplating of magma) metamorphic expulsion rates can be of the same magnitude as thermal convection and thus rapid enough to perturb temperatures and metamorphic grades over broad areas. Thermal anomalies may be present in metamorphic terrains (Ferry, 1992), especially where the efflux is focused in brittle lithologies (Oliver et al., 1990). Isograd patterns could be useful in exploration for deposits precipitated from metamorphically expelled fluids.

Compaction and hydrocarbon maturation cause fluid expulsion that is substantially slower, and there is general agreement that steady flow by these mechanisms cannot produce the thermal anomalies that appear to be associated with many MVT lead–zinc deposits (Cathles and Smith, 1983; Bethke, 1986). This is illustrated by a simple calculation. It was shown in the first section that fluid fluxes of ≥15 m/yr in a 30-m thick aquifer with 1% slope would be reqired to account for the 35°C thermal perturbations associated with the MVT deposits. In the second section it was shown that uniform fluxes from sediments deeper than 3 km due to hydrocarbon maturation or compaction could reach at most ~4×10^{-6} to 4×10^{-5} m/yr. Taking even the most generous geometric flow concentration of 10^4 shown on the right-hand side of Figure 5.6, fluid expulsion rates in the aquifer would still be 40–400 times smaller than the 15 m/yr required to account for the warming during ore deposition.

Further spatial funneling of the discharge could increase the discharge rates, but sufficient funneling to make the formation of these deposits feasible by steady expulsion is unlikely. A possibility—attractive in light of diverse

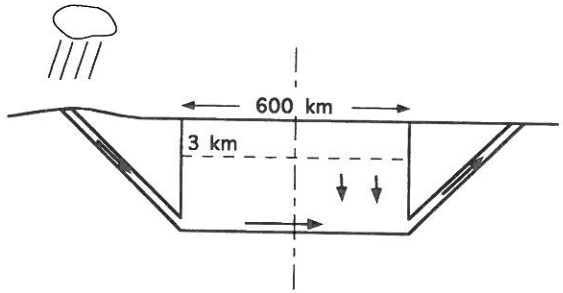

FIGURE 5.6 Idealized basin geometry used for calculations discussed in the text.

evidence of pulses in mineral deposition and minor tectonic disturbances correlated with mineral deposition (Hagni, 1976; Goldhaber et al., 1978; Ohle, 1980; Sverjensky, 1981; Ulrich et al., 1984; Hallager et al., 1990)—is that fluid expulsion from basins is focused in time as well as space and that basins dewater episodically.

For episodic flow, new basin parameters become important. An example is the ratio of the volume of a typical dewatering pulse to the volume of a basin's high-permeability escape network. If the thermal and fluid mass of the escape network is small compared to the thermal and fluid mass of a dewatering pulse, the escape network can be warmed by the pulse, and warm, mineralized fluids can be expelled to near-surface sites of ore deposition. Such a "spitting" basin is favorable to MVT mineralization. If, on the other hand, the thermal and fluid mass in the high-permeability network is large compared to the thermal and fluid mass of a dewatering pulse, the escape channels will not be warmed and expelled fluids (with metals and hydrocarbons) will remain in the basin. This is the "coughing" basin case. A spitting basin will eject hydrocarbons from the basin where they will be bacterially degraded but perhaps still form large but presently subeconomic tar sands like the Athabasca. Hydrocarbons will remain within a coughing basin. The effect of the coughing will be to transfer the hydrocarbons to the most permeable units of the basin, where, after each cough, they may gravitationally migrate upward into traps. The hydrocarbons from many expulsive pulses can thus accumulate in a coughing basin. "Coughing" basins are ideal for hydrocarbon exploration but poor for MVT mineralization; spitting basins are the converse.

A dilemma for the cross-basin, topographic flow hypothesis of MVT mineralization can be illustrated by reference to both the left and right sides of Figure 5.6. The deep Ordovician and Devonian aquifers that fed brines to the classic sites of MVT mineralization in the mid continent of the United States are still filled with brines (Dott and Ginter, 1930; Jorgesen et al., 1986) and the deposits are still very permeable (Weigel, 1965; Bullock, 1973). Once cross-basin, topography-driven flow is established it is not easy to turn off. Flow from the Rocky Mountains to the Ozarks continues today and is still flushing salt from the Great Interior Plains aquifer system through saline springs in Missouri (Banner et al., 1989). The flow is slow, much slower than the 15 m/yr needed for MVT mineralization (Cathles, 1993b). Had the flow been ~15 m/yr, the brines would have quickly been flushed. For example, if the basin in the 600 km × 6 km central part of Figure 5.6 contained 10 vol % evaporites (720×10^{10} g salt in a cross-sectional slice 1 cm wide) and the flow contacted these evaporites sufficiently to maintain salinities in the basal aquifers at 100,000 ppm, a cross-basin hydrologic flow of 15 m/yr in a 30-m wide aquifer system would dissolve the evaporites at the rate of 4.5×10^5 g salt/yr, and the evaporites and brines would be flushed in 16 million years. Salt flushing is a problem for the cross-basin topography-driven flow hypothesis for MVT ore forma-

tion because the basal aquifers in many MVT districts still contain brine (Cathles, 1987, 1993b).

SUMMARY AND CONCLUSIONS

There are many other aspects of heat flow that are important to ore genesis. For example, if episodic flow is important in sedimentary basins it is important to understand how it could occur. Very-low-permeability, capillary (two-phase) seals are probably required. How these are formed and operate may be as important in metamorphic terranes where near-lithostatic pressures are produced as they are in sedimentary basins. The formation and nature of basin seals are currently subjects of active research (Ortoleva, 1994; Whelan, et al., 1994), to which simple thermophysical calculations can contribute. However, enough has been presented to meet the main objective of this chapter, which was to illustrate how simple thermal and flow calculations can be used to investigate the thermal aspects of hydrothermal ore deposition. A compilation has been presented of techniques the author has found useful for estimating the rates and chemical consequences of thermal anomaly migration (deep and near-surface) and for estimating the maximum fluid fluxes that can be expected from various flow mechanisms. The techniques have been illustrated by a number of specific calculations.

The purpose of these examples is not to argue any particular mineralization hypothesis, but to illustrate how calculations are being, and can be, used to help investigate the origins of hydrothermal ore deposits. What makes the study of hydrothermal ore deposits so interesting as well as difficult is that many flow mechanisms may be involved in any one deposit and the combination is usually sufficiently different among deposits that each must be individually considered. It is hoped that the framework and examples presented will encourage geologists to make paper and pencil calculations of other deposits and follow up the sometimes dramatic and unsuspected geological implications with appropriate field investigations. Even (and perhaps especially) in the computer age, simple calculations have an important role to play in ore deposit studies.

ACKNOWLEDGMENTS

I am indebted to The Key Center for Teaching and Research in Strategic Mineral Deposits at the University of Western Australia and in particular to its director, David Groves, for providing the stimulation, place, and time to write this chapter. I thank David Groves and Berkhard Eisenlohr for helpful reviews. I thank H. L. Barnes for advice, comments, and careful editing.

REFERENCES

Baker, E. T., J. W. Lavelle, R. A. Feely, G. J. Massoth and S. L. Walker (1989) Episodic venting of hydrothermal fluids from the Juan de Fuca Ridge: *J. Geophys. Res.* **94**, 9237–9250.

Banner, J. L., and G. N. Hanson (1990) Calculations of simultaneous isotope and trace element variations during water–rock interaction with applications to carbonate diagenesis: *Geochim. Cosmochim. Acta* **54**, 3123–3127.

_____, G. J. Wasserberg, P. F. Dobson, A. B. Carpenter, and C. H. Moore (1989) Isotopic and trace element constraints on the origin and evolution of saline ground waters from central Missouri: *Geochim. Cosmochim. Acta* **53**, 383–398.

Barnes, H. L. (1979) *Geochemistry of Hydrothermal Ore Deposits*: New York: Wiley.

Bear, J. (1972) *Dynamics of Fluids in Porous Media*: New York: American Elsevier.

Behar, E., R. Simonet, and E. Rauzy (1985) A new non-cubic equation of state: *Fluid Phase Equilibria* **21**, 237–255.

Bethke, C. M. (1986) Hydrologic constraints on the genesis of the Upper Mississippi Valley mineral district from Illinois Basin brines: *Econ. Geol.* **81**, 233–249.

_____and S. Marshak (1990) Brine migration across North America—the plate tectonics of groundwater: *Ann. Rev. Earth Planet. Sci.* **18**, 287–315.

_____, J. D. Reed, and D. F. Oltz (1991) Long range petroleum migration in the Illinois Basin: *Am. Assoc. Petrol. Geol. Bull.* **75**, 925–945.

Bischoff, J. L. and R. L. Rosenbauer (1985) An empirical equation of state for hydrothermal seawater (3.2 percent NaCl): *Am. J. Sci.* **285**, 725–163.

Blattner, P. and K. R. Lassey (1989) Stable isotope exchange fronts, Damkohler numbers, and fluid to rock ratios: *Chem. Geol.* **78**, 381–392.

Bredehoeft, J. D., and I. S. Papadopolos (1965) Rates of vertical groundwater movement estimated from the earth's thermal profile: *Water Resour. Res.* **1**, 325–328.

Brikowski, T. and D. Norton (1987) Influence of magma chamber geometry on hydrothermal activity at mid-ocean ridges: *Earth Planet. Sci. Lett.* **93**, 241–255.

Bullock, R. L. (1973) Mine-plant design philosophy evolves from St. Joe's New Lead Belt operations: *Mining Congr. J.* **59**, 20–29.

Burrus, J., A. Kuhfuss, B. Doligez, and P. Ungerer (1991) Are numerical models useful in reconstructing the migration of hydrocarbons? A discussion based on the northern Viking Graben: In: *Petroleum Migration*, W. A. England and A. J. Fleet (eds.). Boulder, CO: Geol. Soc. Am.

Cann, J. R. and M. R. Strens (1989) Modeling periodic megaplume emission by black smoker systems: *J. Geophys. Res.* **94**, 12227–12237.

Carslaw, H. S. and J. G. Jaeger (1959) *Conduction of Heat in Solids*: Oxford: Clarendon Press.

Cathles, L. M. (1977) An analysis of the cooling of intrusives by ground water convection which includes boiling: *Econ. Geol.* **72**, 804–826.

_____(1981) Fluid flow and genesis of hydrothermal ore deposits: *Econ. Geol.* **75th Anniver. Vol.**, 424–457.

_____(1983) An analysis of the hydrothermal system responsible for massive sulfide deposition in the Hokuroku Basin of Japan: *Econ. Geol. Monogr.* **5**, 439–487.

_____(1987) A simple method for calculating temperature perturbations in a basin

caused by the flow of water through thin, shallow-dipping aquifers: *Appl. Geochem.* **2**, 649–655.

——— (1990) Scales and effects of fluid flow in the upper crust: *Science* **248**, 323–329.

——— (1993a) A capless 350°C flow zone model to explain megaplumes, salinity variations, and high temperature veins in ridge axis hydrothermal systems: *Econ. Geol.* **88**, 1977–1988.

——— (1993b) A discussion of flow mechanisms responsible for alteration and mineralization in the Cambrian aquifers of the Ouachita–Arkoma Basin–Ozark system: In: *Diagenesis and Basin Development*, A. D. Horgury and A. G. Robinson (eds.). Tulsa, OK: Am. Assoc. Petrol. Geol. 99–112.

——— and M. E. Shea (1992) Near-field high temperature transport: evidence from the genesis of the Osamu Utsumi uranium mine, Pocos de Caldas alkaline complex, Brazil: *J. Geochem. Explor.* **45**, 565–603.

——— and A. T. Smith (1983) Thermal constraints on the formation of Mississippi Valley-type lead–zinc deposits and their implications for episodic basin dewatering and deposit genesis: *Econ. Geol.* **78**, 783–1002.

Combarnous, M. A. and S. A. Bories (1975) Hydrothermal convection in saturated porous media: In: *Advances in Hydroscience*, V. T. Chow (ed.). New York: Academic Press, pp. 231–307.

Connolly, J. A. D. and A. B. Thompson (1989) Fluid and enthalpy production during regional metamorphism: *Contrib. Mineral. Petrol.* **102**, 347–366.

Coveny, R. M., E. D. Goegel, and V. M. Ragan (1987) Pressures and temperatures for aqueous fluid inclusions in sphalerite for mid-continent country rocks: *Econ. Geol.* **82**, 740–751.

Davis, S. H., S. Rosenblat, J. R. Wood, and T. A. Hewett (1985) Convective fluid flow and diagenetic patterns in domed sheets: *Am. J. Sci.* **285**, 207–223.

De Wiest, R. J. M. (1965) *Geohydrology*: New York: Wiley.

Donaldson, I. G. (1962) Temperature gradients in the upper layers of the earth's crust due to convective water flows: *J. Geophys. Res.* **67**, 3449–3459.

Dott, R. H., and R. L. Ginter (1930) Iso-con map for Ordovician waters. *Am. Assoc. Petrol. Geol. Bull.* **14**, 1215–1218.

Eisenlohr, B. N., L. A. Tompkins, L. M. Cathles, M. E. Barley, and D. I. Groves (1994) Mississippi Valley-type deposits; products of brine expulsion by eustatically induced hydrocarbon generation? An example for northwestern Australia: *Geology* **22**, 315–318.

Elder, J. W. (1966) Heat and mass transfer in the earth: hydrothermal systems: *N. Z. Dept. Sci. Ind. Res. Bull.* **169**, 1–115.

Etheridge, M. A., R. W. R. Rutland, and L. A. I. Wyborn (1987) Orogenesis and tectonic process in the Early to Middle Proterozoic of northern Australia: *Am. Geophys. Union Geodynamics Ser.* **17**, 131–147.

Fehn, U., K. E. Green, R. P. Von Herzen, and L. M. Cathles (1983) Numerical models for the hydrothermal field at the Galapagos spreading center. *J. Geophys. Res.* **88**, 1033–1048.

Ferry, J. M. (1992) Regional metamorphism of the Waits River formation, eastern Vermont: delineation of a new type of giant metamorphic system. *J. Petrol.* **33**, 45–94.

Frape, S. K. and P. Fritz (1987) Geochemical trends from groundwaters from the Canadian Shield: In: *Saline Water and Gases in Crystalline Rocks*, P. Fritz and S. K. Frape (eds.). Memorial Univ., St. Johns, Newfoundland: Geol. Assoc. Canada, Spec. Pap. **33**, pp. 19–38.

Freeze, R. A. and J. A. Cherry (1979) *Groundwater*: Englewood Cliffs, NJ: Prentice-Hall.

Furlong, K. P., R. B. Hanson, and J. R. Bowers (1991) Modeling thermal regimens: In: *Contact Metamorphism*, D. M. Kerrick (ed.). Washington, D.C.: Mineral. Soc. Am., pp. 437–505.

Garven, G. and A. Freeze (1984a) Theoretical analysis of the role of ground water flow in the genesis of stratabound ore deposits: 1. Mathematical and numerical model: *Am. J. Sci.* **284**, 1085–1174.

——— and ——— (1984b) Theoretical analysis of the role of ground water flow in the genesis of stratabound ore deposits: 2. Quantitative results: *Am. J. Sci.* **284**, 1125–1174.

Goldhaber, M. B., R. L. Reynolds, and R. O. Rye (1978) Origin of a South Texas roll-type deposit; II. Sulfur petrology and sulfur isotope studies: *Econ. Geol.* **73**, 1690–1705.

Hagni, R. D. (1976) Tri-State ore deposits: the character of their host rocks and their genesis: In: *Handbook of Stratabound and Stratiform Ore Deposits*, K. H. Wolf (ed.). New York: Elsevier, pp. 457–494.

Halbermehl, M. A. (1984) The Great Artesian Basin, Australia: *BMR J. Australian Geol. Geophys.* **5**, 9–38.

Hallager, W. S., M. R. Ulrich, J. R. Kyle, P. E. Price, and W. A. Gose (1990) Evidence for episodic basin dewatering in salt dome cap rocks: *Geology* **18**, 716–719.

Hanor, J. S. (1979) The sedimentary genesis of hydrothermal fluids: In: *Geochemistry of Hydrothermal Ore Deposits*, H. L. Barnes (ed.). New York: Wiley, pp. 137–172.

Hanson, R. B. (1992) Effect of fluid production on fluid flow during regional and contact metamorphism: *J. Metamorphic Geol.* **10**, 87–97.

Heyl, A. V., M. H. Delevaux, R. E. Zartman, and M. R. Brock (1966) Isotope study of galenas from the Upper Mississippi Valley, the Illinois–Kentucky, and some Appalachian Valley mineral districts: *Econ. Geol.* **61**, 933–961.

Jorgesen, D. G., J. O. Helgesen, R. B. Leonard, and D. C. Signor (1986) Equivalent freshwater head and dissolved-solids concentration of water in rocks of Cambrian, Ordovician, and Mississippian age in the northern midcontinent, U.S.A.: *U.S. Geol. Surv. Miscellaneous Field Study Map, MF-1835B.*

Kadko, D. and W. Moore (1988) Radiochemical constraints on the crustal residence time of submarine hydrothermal fluids: Endeavour Ridge: *Geochim. Cosmochim. Acta* **52**, 659–668.

Labotka, T. C. (1991) Chemical and physical properties of fluids: In: *Contact Metamorphism*, D. M. Kerrick (ed.). Washington, D.C.: Mineral. Soc. Am., pp. 43–104.

Lapwood, E. R. (1948) Convection of a fluid in a porous medium: *Proc. Cambridge Philos. Soc.* **44**, 508–521.

Lassey, K. R. and P. Blatner (1988) Kinetically controlled oxygen isotope exchange between fluid and rock in one-dimensional advective flow: *Geochim. Cosmochim. Acta* **52**, 2169–2175.

Loosveld, R. J. H. and M. A. Etheridge (1990) A model for low-pressure facies metamorphism during crustal thicknening: *J. Metamorphic Geol.* 8, 257–267.

Morton, J. L. and N. H. Sleep (1985) A mid-ocean ridge thermal model: constraints on the volume of axial hydrothermal heat flux: *J. Geophys. Res.* 90, 11345–11353.

Norton, D. L. (1984) Theory and hydrothermal systems: *Ann. Rev. Earth Planet. Sci.* 12, 155–177.

——(1988) Metasomatism and permeability: *Am. J. Sci.* 288, 604–618.

——and L. M. Cathles (1979) Thermal aspects of ore deposition: In: *Geochemistry of Hydrothermal Ore Deposits*, H. L. Barnes (ed.). New York: Wiley, pp. 611–631.

——and J. Knight (1977) Transport phenomena in hydrothermal systems: cooling plutons: *Am. J. Sci.* 277, 937–981.

——and H. P. Taylor (1979) Quantitative simulation of the hydrothermal systems of crystallizing magma on the basis of transport theory and oxygen isotope data: an analysis of the Skaergaard Intrusion: *J. Petrol.* 20, 421–486.

Ohle, E. L. (1980) Some considerations in determining the origin of ore deposits of the Mississippi Valley type: Part II: *Econ. Geol.* 75, 161–172.

Oliver, N. H. S., R. K. Valenta, and V. J. Wall (1990) The effect of heterogeneous stress and strain on metamorphic fluid flow, Mary Kathleen, Australia, and a model for large scale fluid circulation: *J. Metamorphic Geol.* 8, 311–331.

Ortoleva, P. J. (ed.) (1994) Basin Compartments and Seals: Tulsa, OK: *Am. Assoc. Petrol. Geol.* Mem. 61.

Person, M. and G. Garven (1992) Hydrologic constraints on petroleum generation within continental rift basins: theory and application to the Rhine Graben: *Am. Assoc. Petrol. Geol. Bull.* 76, 268–288.

Phillips, G. N., D. I. Groves, and I. J. Brown (1987) Source requirements for the Golden Mile, Kalgoorlie: significance to the metamorphic replacement model for Archean gold deposits: *Can. J. Earth Sci.* 24, 1643–1651.

Polster W. and H. L. Barnes (1994) Comparative hydrodynamic and thermal characteristics of sedimentary basins and geothermal systems in sediment-filled rift valleys: *In*: Basin Compartments and Seals, P. J. Ortoleva (ed.). Tulsa, OK: *Am. Assoc. Petrol. Geol.* Mem. 61, pp. 437–457.

Rich, J. L. (1927) Generation of oil by geologic distillation during mountain building: *Am. Assoc. Petrol. Geol. Bull.* 11, 1139–1149.

Sandiford, M. and R. Powell (1991) Some remarks on high-temperature–low-pressure metamorphism in convergent orogens: *J. Metamorphic Petrol.* 9, 333–340.

Sverjensky, D. A. (1981) The origin of a Mississippi Valley-type deposit in the Viburnum Trend, southeast Missouri: *Econ. Geol.* 72, 339–348.

Ulrich, M. R., J. R. Keyl, and P. E. Price (1984) Metallic sulfide deposits in the Winnfield salt dome, Louisiana: evidence for episodic introduction of metalliferous brines during cap rock formation: *Trans. Gulf Coast Assoc. Geol. Soc.* 34, 435–442.

Uzmann, S. J. (1993) Compilation methods and a preliminary analysis of a regional high resolution geological data compilation within the southern volcanic zone of the Abitibi greenstone belt, Quebec, Canada: M.S. thesis, Department of Geological Sciences, Cornell University.

Weigel, W. W. (1965) The inside story of Missouri's exploration boom—Part 1: *Eng. Mining J.* 166, 77–88.

Whelan, J. K., L. B. Eglinton, and L. M. Cathles, III (1994) Pressure seals—interactions with organic matter, experimental observations, and relation to a "hydrocarbon plugging" hypothesis for pressure seal formation: *In*: Basin Compartments and Seals, P. J. Ortoleva (ed.). Tulsa, OK.: *Am. Assoc. Petrol. Geol.* Mem. 61, pp. 97–117.

Wood, J. R. and T. A. Hewett (1982) Fluid convection and mass transfer in porous sandstones—a theoretical approach: *Geochim. Cosmochim. Acta* 46, 1707–1713.